Optical properties and oxidation of α-phase Ag-Al thin films

Kaludewa S B De Silva[1], Vicki J Keast[2], Angus Gentle[1], and Michael B Cortie[1]*

[1]Institute for Nanoscale Technology, University of Technology Sydney, PO Box 123, Broadway, NSW 2007, Australia

[2]School of Mathematical and Physical Sciences, University of Newcastle, Callaghan, NSW 2308 Australia

*E-mail: michael.cortie@uts.edu.au, tel. +61-9514-2208

Abstract

We investigate a series of Ag-Al thin films containing up to 12 at.% Al with the purpose of discovering whether these alloys would be a better choice for nanophotonic applications than pure Ag. Variable angle spectroscopic ellipsometry, AFM, X-ray diffraction and density functional theory are applied to explore and characterize the materials. Electromagnetic simulations of optical properties are used to place the results into a theoretical framework. We find that the increase in electron-to-atom ratio associated with the Al additions changes the optical properties: additions of the order of 1 to 2 at.% Al are beneficial as they are associated with favorable changes in the dielectric function, but for greater additions of Al there is a flattening of the absorption edge and an increase in optical loss. In addition, contents of more than about 2 at.% Al are associated with the onset of time-dependent intergranular oxidation, which causes a pronounced dip in the reflectance spectrum at about 2.3 to 2.4 eV (~500 to 540 nm).

Keywords: plasmonics, Ag-Al alloys, thin films, optical properties, intergranular oxidation

1. Introduction

The plasmon resonances and other optical properties of the traditional 'coinage metals' (Cu, Ag and Au) have attracted significant scientific interest, motivated by the many actual or potential applications – ranging from spectrally-selective coatings on windows to hybrid opto-electronic devices – that exploit the optical properties of these materials. Gold is popular for these applications due to its oxidation resistance, however its performance in the higher energy half of the visible spectrum is compromised by absorptive loss due to interband transitions of electrons from the *d*-band to higher energy states [1, 2]. The interband transitions cause damping of any localized surface plasmon resonances (LSPRs) or propagating surface plasmon polaritons (SPPs) that have energies matching those of the interband transitions. In contrast, silver, which is also a popular choice for plasmonic applications, exhibits comparatively low loss over the whole of the visible and near infrared (NIR) range but it has relatively lower stability in air and is prone to corrosion on a time scale of weeks to months [3-5]. Alloys between the coinage metals are also of interest [3, 6-8] and it has been shown that, under specific conditions, the alloys $Ag_{0.5}Au_{0.5}$, $Au_{0.1}Cu_{0.9}$ and $Cu_{0.1}Ag_{0.9}$ may be better for plasmonic devices than the pure elements from which they are comprised [8].

Pure Al is also considered to be a 'good' plasmonic material [9-13] and the optical properties of its alloys with the coinage metals has received some attention too. For example, additions of Al to Au have a bleaching effect on the color but increase ε_2 [14] while additions of Al to Cu blue shift the reflectance edge so that $Cu_{0.85}Al_{0.15}$ should show a superior LSPR relative to pure Cu [15]. Here we consider the third option: additions of Al to Ag.

There have been relatively few studies of the Ag-Al system as it is not commonly used in technological applications. In general, additions of Al to Ag are made to improve the latter's thermal stability [16-18]. The phase diagram is relatively complex due to the rather different electronegativity of the two elements. In terms of the Hume-Rothery rules, Al additions (free electron density of 18.1×10^{28} m^{-3}, from its 3*s* and 3*p* orbitals) bring three free electrons per atom compared to the single one of Ag (free electron density of 5.86×10^{28} m^{-3}, from the 5*s* orbital) [19]. This may raise the Fermi level of the alloy or, equivalently, lower its *d*-band, with the result being the blue-shifting of the interband transitions [20]. The extent to which this can be done with the Ag-Al system is constrained, however, by the fact that, under equilibrium conditions, only about 18 at.% Al can be

2

added to the face-centered cubic α-phase terminal solid solution before the solubility limit is exceeded. Additions of Al in excess of the solubility limit lead to the formation of the brittle intermetallic compounds β, δ and μ [21]. This maximum solubility of 18 at.% Al in Ag α-phase occurs at ~500 °C but at room temperature the solubility is even lower, at about 10 at.% Al [21]. The optical properties of the multiphase alloys containing mixtures of the Ag-Al intermetallic compounds have been previously studied by Ng [22]. Finally, at the Al-rich end of the phase diagram, there is an Al-rich fcc α-phase, capable of dissolving of the order of 25 at.% Ag at elevated temperatures [23]. The optical properties of this material have also been studied [24, 25]. In the present paper, however, we limit our investigation to Ag-rich α-phase only.

The properties of Ag-rich Ag-Al α-phase have been only occasionally investigated: Irani *et al*. [26] extracted the dielectric function between 2 and 11 eV (620 nm down to 115 nm) for a range of Al contents, L. Jay Gua *et al.* [17], showed that the addition of Al would dramatically reduce the surface roughness of thin films, Auer *et al*. [27] showed that addition of Al caused the development of a prominent dip in optical reflectance at about 2.0 to 2.3 eV (about 550 to 600 nm) and, most recently, Lee *et al.* [28] showed that addition of up to about 7 at.% Al to Ag caused a systematic increase in plasmon resonance energy of nanoparticles, consistent with an increase in bulk plasma energy brought on by the raised electron density imparted by the Al additions.

The prior work cited above has made it clear that, while addition of Al has some beneficial effects, and can blue-shift plasmon resonances in Ag by 80 nm or so (corresponding to ~0.3 eV at the associated wavelengths), it may also have a disadvantageous effect on optical loss because it increases ε_2 in important regions of the visible spectrum [26, 27]. The two questions that we seek to answer here are (i) whether the increased electron density and hence altered electronic structure of the resultant alloys can bring any advantage for application of these materials in plasmonic devices despite the increase in loss, and (ii) what the relative contributions to the optical properties are from intrinsic factors such as electronic density-of-states and extrinsic factors such as oxidation and surface morphology. In particular, given that some proposed applications of coinage metal nanoparticles are for operation within the 'tissue window' of the human body [29] (~1.3 to 1.8

eV), we will also consider the optical properties in this lower energy range of the spectrum. Importantly, this is below the energy range previously published by Irani *et al*. [26].

2. Experimental and theoretical methods

Thin film samples were made by co-deposition of the pure elements onto clean glass slides or Si wafers using magnetron sputtering under a reduced pressure (0.2 Pa) of Ar. The base pressure of the deposition chamber is about 1.3×10^{-4} Pa. The power applied to each target was varied to provide different ratios of Ag to Al. Sputtering was carried out for about 6 minutes in order to produce films of nearly 200 nm thickness. The substrate was rotated at 12 rev/min and the gap between the target and substrate was approximately 150 mm. Some films were annealed at 300º C for 1 h under vacuum (0.1 Pa) to observe any effects on surface roughness effect or degree of crystallinity.

X-ray diffraction (XRD) was carried out on film samples using a Siemens D5000 X-ray diffractometer and CuKα radiation (1.5406 Å). Energy dispersive spectra of samples of the alloy were obtained using a Zeiss Evo LS15 SEM equipped with a Bruker EDS Quantax 400 at 8 kV. Scanning electron microscope images were taken using 'in lens' mode on a Zeiss Supra 55 VP SEM at 20 kV. The surface morphology of the films was investigated using an AFM (Dimension 3100 with NanoScope IIIA controller) in tapping mode at ambient conditions (scanning speed of 6 microns per second). The AFM images were analyzed using Bruker Nanoscope software, to compute RMS roughness and obtain a 3D image from the topological data.

Optical characterization was carried out in the range of 300 nm - 3000 nm using a V-VASE Ellipsometer by J.A. Woollam Co. and a Perkin Elmer Lambda 950 UV-Vis-IR spectrometer with universal reflectance accessory. The reflectance edge was defined as the wavelength at which dR/dλ was maximum. Analysis of the exposed (top) surface of the sample was generally completed within 30 minutes of removing the freshly deposited sample from the vacuum chamber, so little or no Al_2O_3 would have formed by the time the ellipsometry was completed. Once the optical responses of delta and psi had been measured at multiple angles, a model was developed using the WVASE32 ellipsometric analysis software to extract the dielectric function.

Based on the sputtering rates and time of sputtering it can be predicted that the present films are over 200 nm thickness. The films are quite thick; therefore no transmission data could be collected. The model for the dielectric function was based on a Drude term, two Lorentz oscillators and a pole. An example of the data reduction route is provided as figure S1 in the Multimedia. The model parameters are given in the Multimedia as Table S1.

Our dielectric function for the sample of pure Ag lay between that of Hagemann *et al.* (as presented in the Weaver & Fredericks compilation[30]) and that of Johnson and Christy [31], and was very similar to the Palik [32] data set and reasonably similar to the benchmark data published very recently by Jiang et al.[33] (Multimedia, figure S2). The slight differences are due to surface roughness and grain size [33]. The latter is known to exert a significant effect on the Drude component of the dielectric function of a noble metal [34].

The time-dependent behavior of the samples was assessed by placing a freshly deposited sample into a Janis 600 Cryo chamber mounted on the ellipsometer and then evacuating with a turbo pump. The absolute base pressure of the system was 1.3×10^{-6} Pa. The elapsed time in air prior to evacuation was estimated to be of the order of 30 minutes. This sample was then continuously measured in the ellipsometer for 116 hours under vacuum conditions before, finally, being re-exposed to air again for a further 120 hours.

The DFT calculations were performed using WIEN2K, an all-electron method that includes relativistic effects [35] using the (linearized) augmented plane wave plus local orbitals method (LAPW+lo) method. The generalized gradient approximation (GGA) of Perdew, Burke, and Ernzerhof (PBE) was used for the exchange-correlation potential [36]. The number of *k*-points was set sufficiently high (>50,000) to ensure convergence of the optical properties. The maximum angular momentum for the radial wave functions (*lmax*) was set at 10 and the plane-wave cut-off (*RMTKmax*) was set to 7.0. The complex dielectric function was calculated using the OPTIC routine of WIEN2K [37] in which inter- and intraband transitions are first calculated separately, then summed to obtain the final dielectric function. A broadening parameter of 0.1 eV was applied to the intraband Drude contributions for all of the systems. Further details about our methodology for the calculation of optical properties using WIEN2k may be found elsewhere [38].

The addition of Al to Ag forms a disordered substitutional alloy, however the computational method used here relies on a periodic crystal structure. To model a disordered crystal structure, a suitably sized fcc supercell was constructed and one or more of the Ag atoms replaced with Al. Our previous work on metal alloys has shown that, at these high dilutions, the exact location of the substitutional atoms does not have a significant effect on the optical response [20, 39]. Nevertheless, this assumption was checked using in a 32-atom unit cell containing different arrangements of two Al atoms (equivalent to 6.25 at.% Al). Unit cells were built and visualized with VESTA [40]. The reflectance data calculated using the same input parameters are sufficiently tightly grouped (Multimedia, figure S3) to provide confidence in the methodology used here to represent a random, substitutional solid-solution alloy.

Although WIEN2K can produce a calculated optical reflectance, it is for a perfectly smooth, bulk, surface. The effect of morphological irregularities in the thin films was investigated by calculating reflectance using the discrete dipole approximation. The program DDSCAT v7.3 [41] was used, with the target in a periodic boundary condition so that an infinite 2D film was simulated. The total film thickness was set at 100 nm. Various depths and thickness of a grain boundary film of Al_2O_3 were simulated and the results compared to the measured reflectance to the data to find the best match. The measured dielectric functions of the relevant Ag-Al alloys were used in these calculations. The grain size in these simulations was set at ~60 nm to correspond with the observed surface morphology.

3. Results

This work is motivated by a desire to develop better materials for use in plasmonic devices. As such, the dielectric function is the primary parameter to be considered. Therefore, after first verifying the microstructure of our alloy thin films, we then present their calculated and measured dielectric functions. Durability of the materials is clearly also important and we next investigate the time-dependent oxidation of the surfaces of these materials. Finally, in the Discussion section, we analyze the merits of these alloys for plasmonic applications.

The chemical compositions of the films were confirmed by EDS. XRD patterns were obtained on as-deposited films of different compositions, figure 1. All the peaks could be indexed on a face-centered cubic unit cell with the space group Fm3m [21], proving that the investigated composition range lay within the $(Ag)_{fcc}$ terminal solid solution at the Ag end of the Ag-Al phase diagram. Since these patterns were collected on films, factors such as residual stress state [18], preferred orientation, small grain size and thickness will result in broad XRD peaks and some scatter in estimated value of the lattice parameter. Nevertheless, Rietveld analysis of the patterns indicated that the lattice parameter of these alloys was essentially unchanged at 0.4082 ± 0.0001 nm, which is within the scatter band of values (0.4079 ± 0.0006 nm) reported for pure Ag in the JC-PDF and other databases. This is the expected result for a random substitutional solid solution as the metallic radii of the Al and Ag atoms are very similar (0.1445 vs 0.1432 nm) [42].
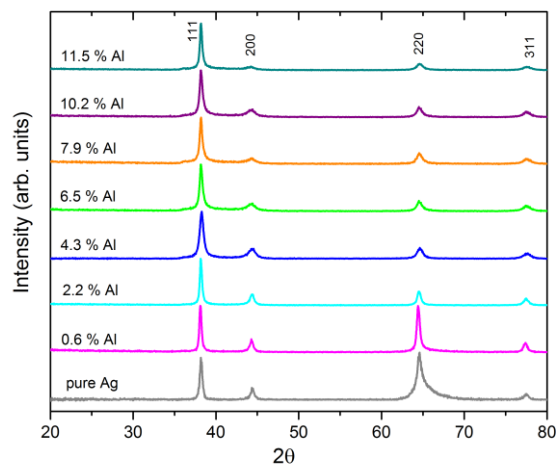

Figure 1: XRD patterns of Ag and the series of $Ag_{1-x}Al_x$ solid solutions. All the peaks can be indexed as belonging to the fcc structure, therefore the investigated range of solid solutions lies within the α-(Ag) terminal solid solution.

The complex dielectric function of non-magnetic materials can be expressed as,

$$\varepsilon(\omega) = \varepsilon_1(\omega) + i.\varepsilon_2(\omega) \tag{1}$$

where ε is the dielectric function and ω is the frequency of the light. Figure 2 shows the calculated and experimental results for the real part of the dielectric functions (ε_1) for $Ag_{1-x}Al_x$ ($0<x<0.125$), measured on freshly deposited films. Our measured data for pure Ag are essentially identical to those in the literature (Multimedia, figure S2). Data from Irani *et al.*[26] for 8.1 Al % was extracted from the original work by digitizing a figure and is plotted as a dashed line for comparison. In the spectral regions where they overlap, our data is in reasonable agreement with that of Irani *et al.*

To place these results into context, it is useful to note that a localized plasmon resonance on a nanosphere in air or vacuum requires, in the quasistatic limit, that $\varepsilon_1 = -2$ [43, 44], which, in these samples, is achieved at an energy of 3.49 eV for the pure Ag, falling to 3.45 eV at 2 % Al, and then rising to 3.76 eV for the 11.5 at.% Al alloy, figure 3. Data from the DFT calculations are also plotted in figure 3. The trends for *ab initio* and experimental data are qualitatively similar and support each other: both show that the resonance of a nanosphere is at first red-shifted and then blue-shifted as Al additions are made. These shifts arise from the introduction of two additional interband transitions due to the Al addition. When Al is first added, a large number of new interband transitions at low energy immediately appear. This is probably because the added Al electron states have *p*-character, meaning that they can undergo transitions into the unoccupied Ag *s* states, which previously were not accessible from the occupied Ag *s* and *d* states. This changes the nature of the dielectric function so that ε_2 becomes higher at low energies (<2 eV) and the $\varepsilon_1(\omega)$ line is blue-shifted overall. This causes the resonance to decrease in energy. At higher Al contents, a new interband transition appears at ~ 2.5eV which reverses this trend.
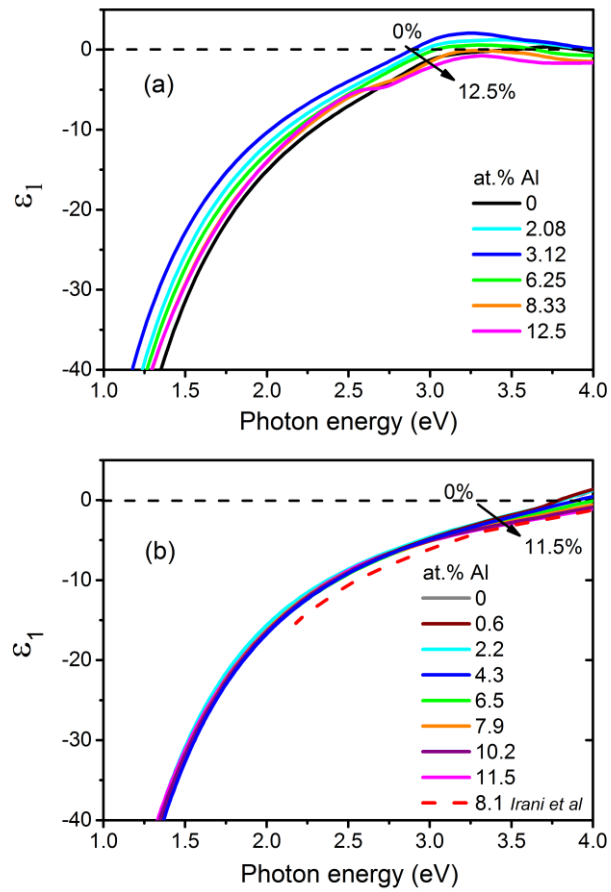
Figure 2. Real part of dielectric functions of Ag-rich Ag-Al α-phase. (a) Calculated by DFT, and (b) measured data.
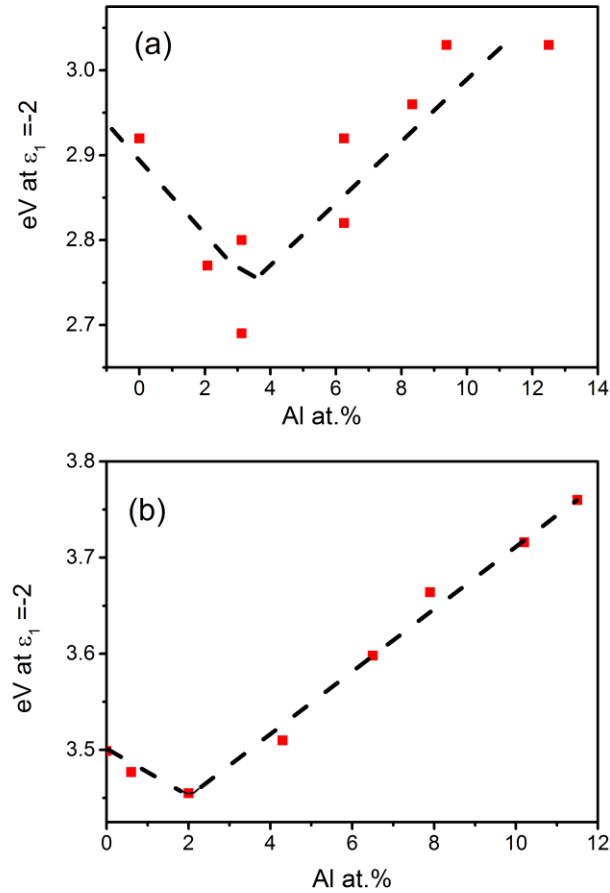
Figure 3. The relationship between photon energy at which $\varepsilon_2=-2$, and the Al level, showing that the nominal energy of a nanosphere resonance is at first red-shifted by additions of up to 2 or 3% Al, then blue-shifted for greater additions. (a) Results from DFT calculations, showing some repeat calculations for different atomic configurations, (b) measured data. Lines drawn to guide the eye only.

The imaginary part (ε_2) of the complex dielectric functions is related closely to the loss at that photon energy. Optical losses can be greatly affected by electron scattering caused by surface imperfections such as surface roughness, porosity and grain boundaries, along with the losses due to interband and intraband transitions. Although the extrinsic losses due to the surface imperfections can be controlled through preparation methods, damping due to intrinsic metallic losses cannot be reduced unless the electronic structure is altered [46]. Figure 4 shows the imaginary part of the dielectric functions of the thin films, measured on as-deposited films. Unfortunately, ε_2 increases with increasing Al levels. However, small addition levels *i.e.* < 2 at.%, have little effect on the imaginary permittivity of this alloy system. The ε_2 values found by Irani *et al.* are also shown and

lie very close to our data. The onset of the interband adsorption is associated with transitions from the top of the *d*-band to states just above the Fermi level [47]. The interband adsorption can be identified in plots of dielectric functions as an inflection at around 3.8 eV for silver [45] and is visible in our experimental data. In contrast, the expected blue-shifting of the onset point is harder to see because our measurements do not go above 4.15 eV. The absorption edge provided by the DFT results lies lower in energy by about 1 eV. This offset in energy between DFT and experimental results is usual when the CGA approximation and the random phase approximation are used (see Experimental and theoretical methods section) [48-51]. Generally, however, the form of the dielectric function calculated with DFT is qualitatively correct even if the energies are offset.
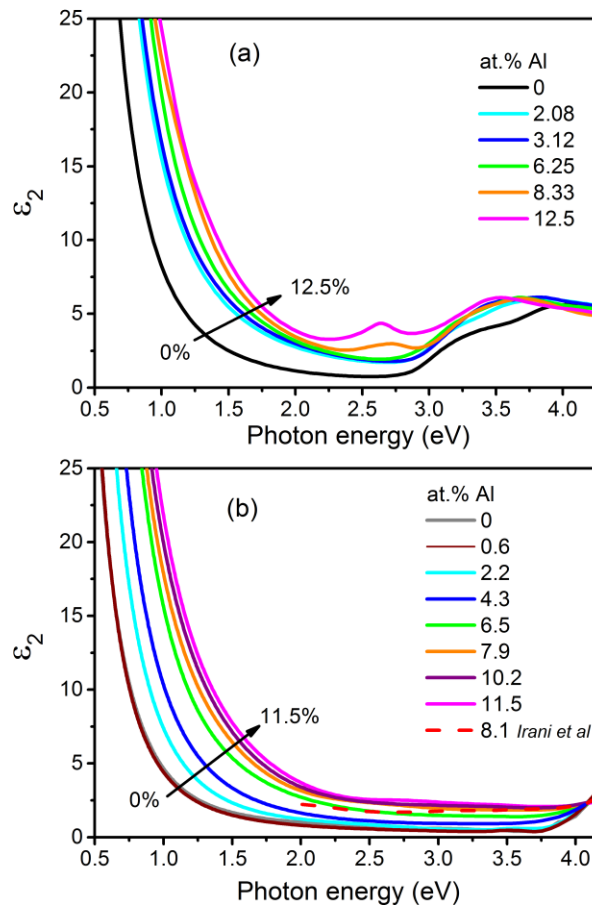

Figure 4. Imaginary part of the dielectric functions of Ag and Ag$_{1-x}$Al$_x$ solid solution. (a) Calculated by DFT, (b) measured. The data of Irani *et al*.[26] for 8.1 Al % are plotted as a dashed line for comparison on (b) for comparison and were obtained by measurement off the original figures. The energy of the absorption edge calculated by DFT is about 1 eV less than the actual edge (see text).

Unlike Cu and Au, the reflection edge of Ag is at the high energy end of the visible spectrum [3] (around 3.9 eV), ensuring that the element has an almost white color. Also, whereas the reflectance edge of Cu or Au is due to the onset of interband transitions, the reflectance edge in Ag is also connected to the reflectivity dip associated with the bulk plasmon energy. The reflectance spectra calculated by DFT and those calculated from the measured dielectric function are shown in figure 5(a) and 5(b) respectively. In the experimental data, the reflectance edge is not moved much by additions of Al; instead the slope of the edge is decreased monotonically with Al content. In contrast, the results from DFT appear to show some non-linearity: the reflectance edge starts at 2.93 eV for pure Ag, is red-shifted to about 2.80 eV by an additions of 3.1 at.% Al, after which it is blue-shifted back to about 2.95 eV by an addition of 8.3 at.% Al. One reason for the difference between the two is the fact that the DFT calculations shown in the figure sample only a single atomic configuration per Al level. In contrast, the experimental data incorporate all possible atomic configurations of the designated level of Al in Ag. Overall, however, it is clear that addition of Al to Ag causes a smearing out the interband transitions responsible for causing the reflectance edge, either by the creation of lower energy transitions than for pure Ag and/or by additional scattering processes introduced by the Al atoms in the lattice. This becomes quite evident in the DFT calculations for 12.5 at.% Al, for which the calculated reflectance shows a 'shelf' in the reflectance spectrum at about 2.68 eV. This latter effect is a specific contribution from the interband transitions of Al. Overall, the present data and those in the prior literature [26, 28] confirm that large additions (> 3 at.%) Al to Ag causes a blue-shift in the photon energies at which a LSPR on sphere would be possible. The shift is about +0.023 eV per atom percent Al added.

Re-measurement of the reflectance spectra after 8 months had passed revealed that some Al-containing samples had developed a pronounced dip at about 2 eV, figure 5(c). For example, the dip at ~2 eV causes about 20% absorption in the alloy with 6.5 at.% Al compared to pure Ag. This effect was absent from the pure silver samples. Therefore, the question is whether it was an extrinsic artefact caused by the occurrence of oxidation to form Al_2O_3 or an intrinsic effect due to an altered band structure of the Al-containing alloys. This dip has been commented on before by Auer *et al*. [27] who attributed it to grain boundary defects. The dip is clearly absent from our DFT results for the unit cells containing a single Al atom although simulations of *clusters of Al* within

the Ag$_{1-x}$Al$_x$solid solution did reproduce a reflectance with a feature similar to the dip (Multimedia, figure S4). In principle, therefore, precipitation of Al-rich clusters could provide an intrinsic, time-dependent explanation for the dip as an alternative explanation to oxidation.
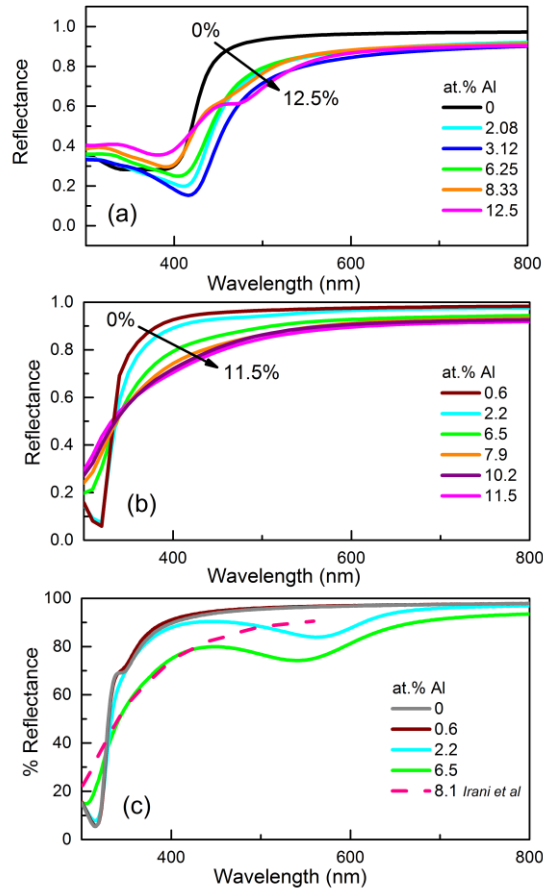

Figure 5. Reflectance of Ag and Ag$_{1-x}$Al$_x$ solid solution, (a) DFT calculations, (b) reflectance extracted from ellipsometry data collected on freshly sputtered samples (c) Reflectance of Ag and Ag$_{1-x}$,Al$_x$ solid solution, measured after 8 months. The data of Irani *et al*.[26] for 8.1 Al % are plotted as a dashed line for comparison.

Further work was therefore conducted to resolve the issue of whether the time-dependent appearance of the dip was due to oxidation (an extrinsic effect) or clustering of Al atoms (an intrinsic effect). Backside (through the glass substrate) measurements on aged films did not show any sign of the 2 eV dip. This observation strongly suggested that the dip was due to some extrinsic effect like oxidation or surface roughness

13

that affected only the exposed surface of the films. We confirmed this by preparing a fresh film (4.5 at.% Al) on Si, and immediately transferring it to a vacuum chamber mounted on the ellipsometer. For ease of viewing the changes to the films, we show the subsequent *calculated* reflectance, based upon the measured ellipsometry measurements. Figure 6(a) presents the reflectance of the film with time, measured under vacuum conditions. The film showed no dip when it was under vacuum, even after 120 hours. Once the sample was exposed to air, however, there was an immediate response, with the development of a reflectance dip at about 2 eV, figure 6(b). The data can be processed to extract the ostensible extinction k (from $m=n+ik$) at 540 nm, figure 6(c). A rapid initial change in k when the vacuum is broken is clearly visible, as is the subsequent ongoing slow change in k with time.
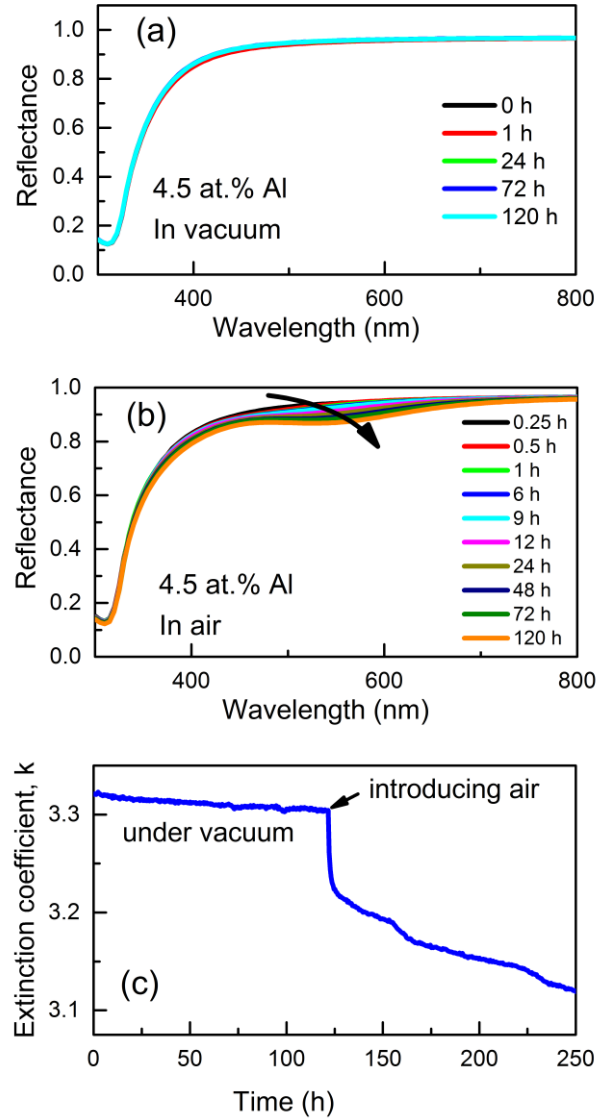
Figure 6. (a) Reflectance of $Al_{0.045}Ag_{0.955}$ film deposited on Si wafer, measured under vacuum, displaying no significant changes of the measurements for 120 h. (b) Reflectance of the same film measured in air, displaying significant changes in reflectance curves collected over 120 h. (c) Extinction coefficient, k of the same film showing the sudden drop when exposed to air.

Annealing of the samples removed the dip at ~2 eV but created a new one at about ~3 eV (Multimedia, figure S5) as reported previously by Auer et al. [27] Surface morphology was rougher after annealing which could be due to Ag clustering. [52][53]An AFM study was carried out on some films over a scan size 5 μm × 5

μm to investigate a possible relationship between roughness and the observation of the dip. Figure 7(a)-(c) shows the 3D AFM surface morphologies of films of pure Ag, 0.6 and 2.2 Al at.% respectively. As evidenced by the AFM images shown in figure 7 and the root mean square (RMS) values, it is clear that adding Al in small quantities facilitated the production of a smoother film. Similar observations have been reported by Gu *et al.* [17], who attributed that to restraining the expansion of Ag particles during the film growth. They further reported on formation of a capping layer of Al_2O_3 due to inward diffusion of O and outward diffusion of Al resulting in a reduction of 4 at.% Al from the surface within few minutes, which, they claimed, caused an improvement in the thermal stability of the film. However, in our case, thin films with greater than ~6 at % of Al showed a severely corroded appearance after several weeks exposure to air, indicating poor stability of the films. Annealing the samples *increased* their roughness considerably (Multimedia, figure S6).
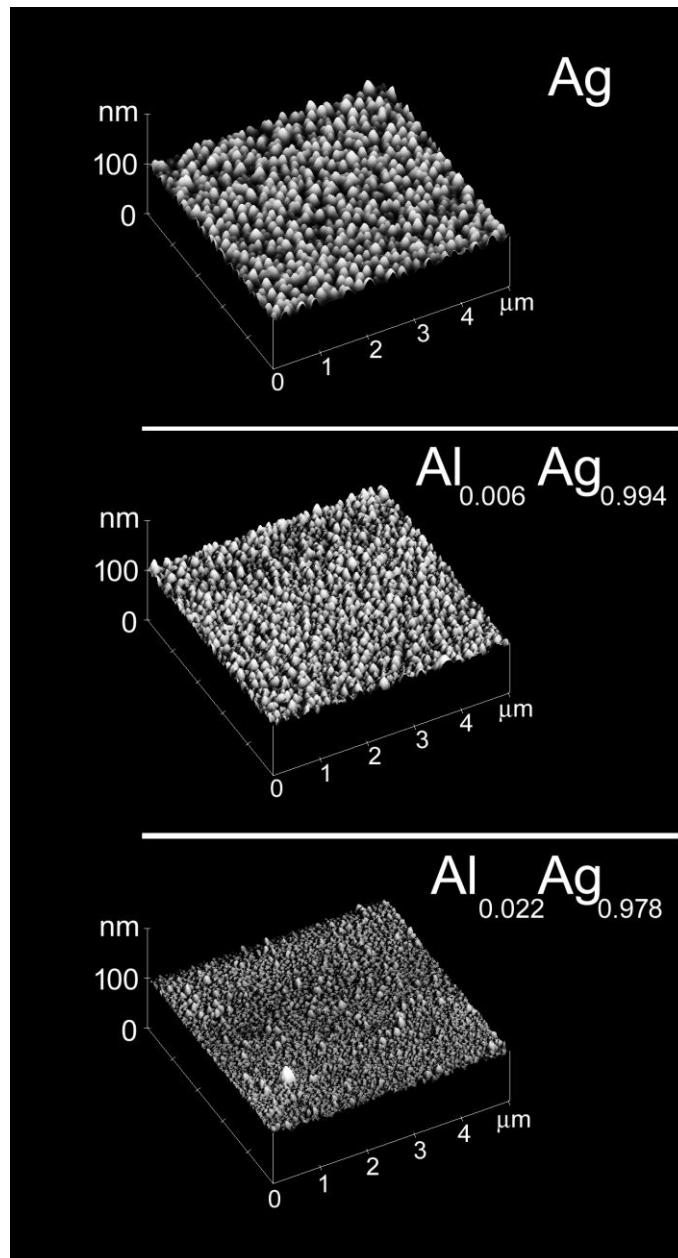
Figure 7. (a)-(c) Surface morphology by AFM 3D images, showing the smoothing due to Al additions. The RMS roughness values of pure Ag, $Ag_{0.994}Al_{0.006}$ and $Ag_{0.978}Al_{0.022}$ are 6.07, 4.10 and 2.34 nm respectively.

The shape of the reflectance curve could not be reproduced with electromagnetic simulations based on a continuous top film of Al_2O_3, however introduction of the Al_2O_3 as a *grain boundary* film produced the required dip feature. It is reasonable to attribute the formation of such a film as being due to the diffusion of ambient oxygen down the grain boundaries and its *in situ* reaction there with Al. Diffusion down grain boundaries is generally an order of magnitude faster than diffusion through the bulk crystal due to the disordered nature of the

17

lattice at grain boundaries and the resulting intergranular oxidation is a well-known phenomenon in many alloy systems. The changes in reflectance that follow may be due to increasing penetration and thickening of the intergranular film, with the rate-controlling process in the latter case being the lateral diffusion of Al into the crystalline interior of the grains. The effect of the thickness and depth of a grain boundary film of Al_2O_3 on the reflectance was tested by performing electromagnetic simulations on various morphologies of thin film. In figure 8 the effect of the depth and thickness of the grain boundary film of Al_2O_3 is evaluated for the Ag-4.5 % Al and Ag-6.5% Al alloys. Clearly, the onset of the dip can be closely reproduced by introducing a small amount of intergranular oxidation. It was found that the photon energy at which a dip occurred was closely correlated to the ratio of depth to width of the grain boundary, whilst the reflectance minimum in the dip was mostly dependent on the volume of grain boundary oxide. An empirical model was fitted to the results of the simulations and indicated that the dip observed in the 4.5 % Al after 5 days exposure to air could be explained, to a first approximation, by a grain boundary films of 3.5 nm depth by 2.5 nm width. The corresponding values for the 6.5 % Al sample after 8 months exposure were 5.8 nm depth and 4.0 nm width. The sample surface was made perfectly smooth in this simulation but of course there will likely also be some further influence of surface roughness on the shape of the reflectance spectrum.
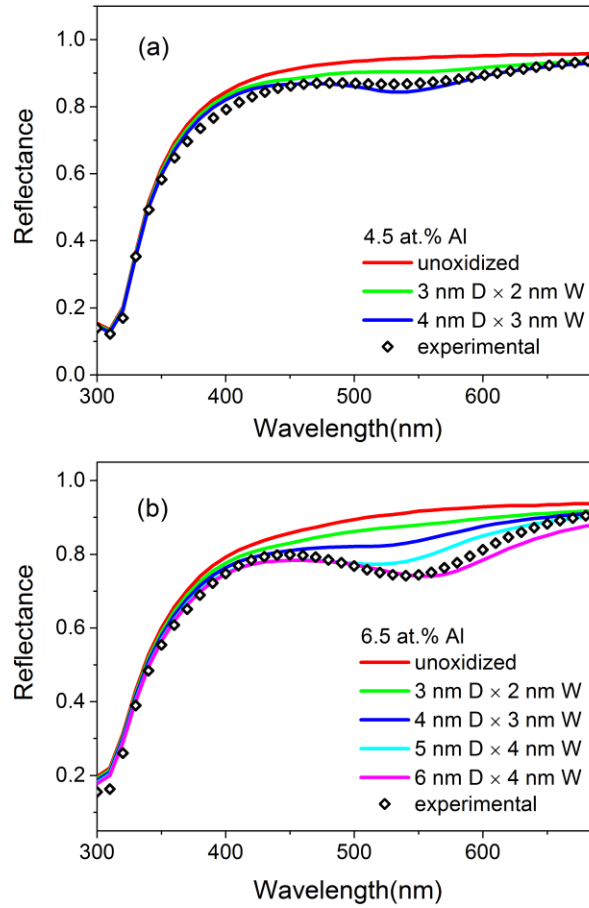
Figure 8. Calculated reflectances of a series of 100 nm thick films containing increasing depths and widths of grain boundary oxidation for Ag-4.5 at.% Al and Ag-6.5 at.% Al. The experimental data also plotted for comparison. Experimental data presented for 4.5 at.% Al was collected after 120 h exposure to air while data for Ag-6.5% Al was collected after 8 months exposure to air.

4. Discussion: suitability of Ag-rich α -(Ag,Al) alloys for plasmonic applications

The relationship between real and imaginary permittivities of the materials can be used as a guide to finding the optimal operating conditions and the right geometry for a localized surface plasmon resonance (LSPR). Their effects on the LSPR can be conceptually separated so that ε_1 represents the operating point (resonance frequency) and ε_2 represents the loss [44]. In figure 9(a) the effect of Al addition on the relationship between ε_1 and ε_2 is explored. These plots indicate that up to a 1 at.% Al addition to Ag is not harmful to the dielectric

function. However, performance is decreased for larger Al additions, making such alloys less suitable for plasmonic applications in the measured energy range. A variety of other metrics have been proposed in the literature [44]. In figure 9(b) we show the 'loss function'. The general conditions for plasma oscillations at a frequency Ω can be expressed as $\Omega = \omega_p - i\Gamma$, where ω_p is the plasma frequency and Γ refers to the damping of the plasma oscillations. This value is equal to zero at the existence of plasma oscillations. When the damping is very small, the conditions for the plasma can be written as $\varepsilon_1(\omega_p) = 0$. In practice, plasma resonance can be identified at the maximum in loss function which is defined as $Im(-1/\varepsilon) = \varepsilon_2 /(\varepsilon_1^2 + \varepsilon_2^2)$ [45, 54]. As predicted by the theory, it shows a sharp peak at about 3.8 eV for Ag and low Al alloyed solid solutions, however, the sharpness reduces when the Al additions are increased. Increased electron density alone should not be harmful so we deduce that the problem with greater Al additions is one of greater electron scattering due to compositional disorder in the system.
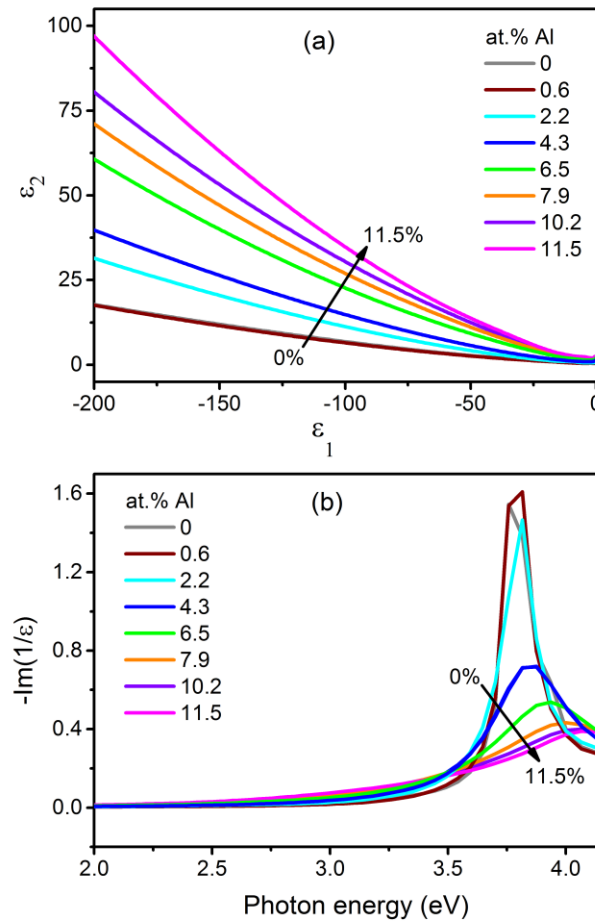
Figure 9. Performance of $Ag_{1-x}Al_x$ alloys in plasmonic applications, (a) Imaginary permittivity *vs.* real permittivity of Ag-rich α-phase solid solutions. (b) Loss function of Ag-rich α-phase solid solutions.

5. Conclusions

We have investigated the optical properties of the terminal $Ag_{1-x}Al_x$ solid solution ($0 < x < 0.12$) in the Ag-Al binary system. Due to the similarity of atomic radii, there is almost no change in lattice parameter across the phase field, however, addition of Al causes a systematic increase in the electron-to-atom ratio of from 1.00 to about 1.23. Additions of up to about 2 or 3 at.% Al cause a red-shift in the localized surface plasmon resonances calculated for an alloy nanosphere, but this trend reverses for greater amounts of Al, and these cause a significant blue shift in the resonant frequency. The evidence indicates that a small additions of Al, of the order of 1 to 2 at.%, are beneficial as they reduce surface roughness and do not have an adverse effect on optical loss.

However, higher alloying levels are deleterious due to an altered band structure which is associated with greater loss. Aluminum additions are associated with a time- and environment-dependent process that generates an absorption peak at about ~2 eV / 600 nm. Intergranular oxidation seems the most likely culprit. Clearly, the relatively small amounts of Al added to these alloys are insufficient to allow for the development of a continuous protective oxide film in the as-deposited samples.

Multimedia: Ellipsometry data for the 6.5 at% Al film, dielectric function of Ag from various sources, results of density functional theory calculations of the reflectance for 6.25 at.% Al alloy, experimental reflectance and X-ray diffraction patterns of films before and after annealing, atomic force microscopy images of surface of films after annealing. This material is available free of charge via the Internet at **

REFERENCES

[1]   Naik, G. V., Shalaev, V. M. and Boltasseva, A. 2013 Alternative plasmonic materials: beyond gold and silver *Adv. Mater.* **25** 3264-94.

[2]   Keast, V. J., Zwan, B., Supansomboon, S., Cortie, M. B. and Persson, P. O. Å. 2013 $AuAl_2$ and $PtAl_2$ as potential plasmonic materials *J. Alloys Compd.* **577** 581-6.

[3]   West, P. R., Ishii, S., Naik, G. V., Emani, N. K., Shalaev, V. M. and Boltasseva, A. 2010 Searching for better plasmonic materials *Laser & Photon. Rev.* **4**(6) 795-808.

[4]   Keast, V. J., Myles, T. A., Shahcheraghi, N. and Cortie, M. B. 2016 Corrosion processes in bulk silver and in triangular silver nanoparticles *J. Nanoparticle Res.* **18**(2) 18-45.

[5]   Pillai, S., Disney, C. E., Yang, Y. and Green, M. A. 2015 The effect of ageing on the scattering properties of silver nanoparticles for a plasmonic solar cell *J. Appl. Phys.* **118** 153102.

[6]   Cortie, M. B. and McDonagh, A. M. 2011 Optical properties of hybrid and alloy plasmonic nanoparticles *Chem. Rev.* **111**(6) 3713–35.

[7]   Rioux, D., Vallières, S., Besner, S., Muñoz, P., Mazur, E. and Meunier, M. 2014 An analytic model for the dielectric function of Au, Ag, and their alloys *Adv. Optical Mater.* **2** 176–82.

[8]   Gong, C. and Leite, M. S. 2016 Noble metal alloys for plasmonics *ACS Photonics* **3** 507−13.

[9]   Knight, M. W., King, N. S., Liu, L., Everitt, H. O., Nordlander, P. and Halas, N. J. 2014 Aluminum for plasmonics *ACS Nano* **8**(1) 834–40.

[10]   Chong, X., Jiang, N., Zhang, Z., Roy, S. and Gord, J. R. 2013 Plasmonic resonance-enhanced local photothermal energy deposition by aluminum nanoparticles *J. Nanopart. Res.* **15**(6) 1678.

[11]   Ekinci, Y., Solak, H. H. and Löffler, J. F. 2008 Plasmon resonances of aluminum nanoparticles and nanorods *J. Appl. Phys.* **104**(8) 083107.

[12]   Liu, J., Cankurtaran, B., McCredie, G., Ford, M., Wieczorek, L. and Cortie, M. 2005 Investigation of the optical properties of hollow aluminum 'nano-caps' *Nanotechnology* **16** 3023-8.

[13]   Liberman, V., Diest, K., Stull, C. W., Cook, M. T., Lennon, D. M., Rothschild, M. and Schoeche, S. 2016 Wafer-scale aluminum nanoplasmonic resonators with optimized metal deposition *ACS Photonics* **3** 796−805.

[14]   Silva, K. S. d., Keast, V. J. and Cortie, M. B. 2016 Effect of Al additions on the optical properties of Au α-phase *J. Alloys & Compounds* **679** 225-30.

[15]   Shahcheraghi, N., Gentle, A., Arnold, M., Keast, V. J. and Cortie, M. B. 2016 Anomalously strong plasmon resonance in aluminum bronzes by modification of the electronic density-of-states *J. Phys. : Cond. Matt.* **28**(40) 405501.

[16]   Kim, J.-Y., Na, S.-I., Ha, G.-Y., Kwon, M.-K., Park, I.-K., Lim, J.-H., Park, S.-J., Kim, M.-H., Choi, D. and Min, K. 2006 Thermally stable and highly reflective AgAl alloy for enhancing light extraction efficiency in GaN light-emitting diodes *Appl. Phys. Lett.* **88**(4) 043507.

[17]   Gu, D., Zhang, C., Wu, Y.-K. and Guo, L. J. 2014 Ultrasmooth and thermally stable silver-based thin films with subnanometer roughness by aluminum doping *ACS Nano* **8**(10) 10343–51.

[18]   Ali, M. K. M., Ibrahim, K. and Mkawi, E. M. 2013 Ag-Al alloy thin film on plastic substrate by screen printing for solar cell back contact application *Mater. Sci. in Semiconductor Process.* **16**(3) 593-7.

[19]   Ashcroft, N. W. and Mermin, N. D. 1976 *Solid State Physics*, (New York: Harcourt College Publishers,).

[20]   Keast, V. J., Birt, K., Koch, C. T., Supansomboon, S. and Cortie, M. B. 2011 The role of plasmons and interband transitions in the color of $AuAl_2$, $AuIn_2$ and $AuGa_2$ *Appl. Phys. Lett.* **99**(11) 111908.

[21]   McAlister, A. J. 1987 The Ag−Al (silver-aluminum) system *Bull. Alloy Phase Diagrams* **8**(6) 526-33.

[22]   Ng, M. W. 1994, *Angular Selective Window Coatings* (PhD, Dept. of Applied Physics, Sydney: University of Technology Sydney).

[23]   Baker, H. and Okamoto, H. 1992 *Alloy Phase Diagrams*, Vol. 3 (Materials Park: ASM International).

[24]   Villanucci, D. P., Teng, Y. Y. and Karakashian, A. S. 1974 Surface plasma oscillations on disordered binary alloy surfaces *Phys. Lett.* **50A**(1) 39-41.

[25]   Yang, G., Fu, X. J., Sun, J. B. and Zhou, J. 2013 Optical properties of aluminum silver alloy films deposited by magnetron sputtering *J. Alloys Compounds* **547** 23-8.

[26]   Irani, G. B., Huen, T. and Wooten, F. 1971 Optical properties of Ag and α-phase Ag-Al alloys *Phys. Rev. B* **3**(8) 2385-90.

[27]   Auer, S., Wan, W., Huang, X., Ramirez, A. G. and Cao, H. 2011 Morphology-induced plasmonic resonances in silver-aluminum alloy thin films *Appl. Phys. Lett.* **99**(4).

[28]   Lee, D.-J., Yim, H.-D., Kim, Y.-G., Jeong, Y.-B., Kim, T. Y., Hwangbo, C. K., Jun, Y. C., Park, S.-G., Lee, S.-G. and O, B.-H. 2013 Resonant wavelength tuning of localized plasmons in silver-aluminum nanoparticles *J. Korean Physical Soc.* **63**(11) 2098-101.

[29]   Simpson, C. R., Kohl, M., Essenpreis, M. and Copey, M. 1998 Near-infrared optical properties of *ex vivo* human skin and subcutaneous tissues measured using the Monte Carlo inversion technique *Phys. Med. Biol.* **43** 2465–78.

[30]   Weaver, J. H. and Frederikse, H. P. R., in *CRC Handbook of Chemistry and Physics*, (Ed: D. R. Lide), CRC Press, Boca Raton **2001**, 133.

[31]   Johnson, P. B. and Christy, R. W. 1972 Optical constants of the noble metals *Phys. Rev. B* **6**(12) 4370-9.

[32]   Palik, E. D. 1998 *Handbook of Optical Constants of Solids*, Vol. 1 (San Diego: Academic Press).

[33]   Jiang, Y., Pillai, S. and Green, M. A. 2016 Realistic silver optical constants for plasmonics *Sci. Rep.* **6** 30605.

[34]   Chen, K.-P., Drachev, V. P., Borneman, J. D., Kildishev, A. V. and Shalaev, V. M. 2010 Drude relaxation rate in grained gold nanoantennas *Nano Lett* **10** 916–22.

[35]   Blaha, P., Schwarz, K., Madsen, G. K. H., Kvasnicka, D. and Luitz, J. 2001 *WIEN2k, An Augmented Plane Wave + Local Orbitals Program for Calculating Crystal Properties* (Vienna, Austria: Techn. Universität Wien).

[36]   Perdew, J. P., Burke, S. and Ernzerhof, M. 1996 Generalized gradient approximation made simple *Phys. Rev. Lett.* **77** 3865-8.

[37]   Ambrosch-Draxl, C. and Sofo, J. O. 2006 Linear optical properties of solids within the full-potential linearized augmented planewave method *Comp. Phys. Comm.* **175** 1.

[38]   Keast, V. J. 2013 An introduction to the calculation of valence EELS: Quantum mechanical methods for bulk solids *Micron* **44** 93-100.

[39]   McPherson, D. J., Supansomboon, S., Zwan, B., Keast, V. J., Cortie, D. L., Gentle, A., Dowd, A. and Cortie, M. B. 2014 Strategies to control the spectral properties of Au-Ni thin films *Thin Solid Films* **551** 200-4.

[40]   Momma, K. and Izumi, F. 2011 VESTA 3 for three-dimensional visualization of crystal, volumetric and morphology data *J. Appl. Cryst.* **44** 1272-6.

[41]   Draine, B. T. and Flatau, P. J. 2008 The discrete dipole approximation for periodic targets: I. Theory and test *J. Opt. Soc. Am. A* **25**(11) 2693-703.

[42]   Teatum, E., Gschneidner, K. and Waber, J. 1960, *Compilation of Calculated Data Useful in Predicting Metallurgical Behaviour of the Elements in Binary Alloy Systems*, Report LA-2345 (Los Alamos Scientific Laboratory, California, USA).

[43]   Stockman, M. I. 2011 Nanoplasmonics: past, present, and glimpse into future *Optics Express* **19**(22) 22029-106.

[44]   Arnold, M. D. and Blaber, M. G. 2009 Optical performance and metallic absorption in nanoplasmonic systems *Optics Express* **17**(5) 3835-47.

[45]   Ehrenreich, H. and Philipp, H. 1962 Optical properties of Ag and Cu *Phys. Rev.* **128**(4) 1622.

[46]   Blaber, M. G., Arnold, M. D. and Ford, M. J. 2010 A review of the optical properties of alloys and intermetallics for plasmonics *J. Phys.: Condens. Matter* **22**(14) 143201.

[47]   Keast, V. J. and Bosman, M. 2008 Applications and theoretical simulation of low-loss electron energy-loss spectra *Mater. Sci. Technol.* **24**(6) 651-9.

[48]   De Silva, K. S. B., Gentle, A., Arnold, M., Keast, V. J. and Cortie, M. B. 2015 Dielectric function and localized plasmon resonances of equiatomic Au-Cu *J. Phys. D: Appl. Phys.* **48** 215304.

[49]   Marini, A., Onida, G. and DelSole, R. 2002 Quasiparticle electronic structure of copper in the GW approximation *Phys. Rev. Lett.* **88** 016403.

[50]   Marini, A., DelSole, R. and Onida, G. 2002 First-principles calculation of the plasmon resonance and of the reflectance spectrum of silver in the GW approximation *Phys. Rev. B* **66** 115101.

[51]   Alkauskas, A., Schneider, S. D., Hébert, C., Sagmeister, S. and Draxl, C. 2013 Dynamic structure factors of Cu, Ag, and Au: Comparative study from first principles *Phys. Rev. B* **88** 195124.

[52]   Drachev, V. P., Chettiar, U. K., Kildishev, A. V., Yuan, H.-K., Cai, W. and Shalaev, V. M. 2008 The Ag dielectric function in plasmonic metamaterials *Optics Express* **16**(2) 1186-95.

[53]   Rizzo, A., Tagliente, M. A., Alvisi, M. and Scaglione, S. 2001 Structural and optical properties of silver thin films deposited by RF magnetron sputtering *Thin Solid Films* **396** 29-35.

[54]   Yang, G., Sun, J. and Zhou, J. 2011 Dielectric properties of aluminum silver alloy thin films in optical frequency range *J. Appl. Phys.* **109**(12).